6

SOLID EARTH MODELLING PROGRAMME

Solid Earth Modelling group research activities are multidisciplinary (Engineering and Earth Sciences) and multi-component (GNSS Geodesy, computational seismology, geology, geophysics, physics and modelling). Major focus of the group is data analysis and modelling to gain significant insights in to sub-surface process in the earth's crust. During the year 2014-2015 group has contributed to preliminary estimation of crustal structure beneath Kashmir Himalayas, probabilistic earthquake hazard maps for South India, site response study of Bangalore city, reflection and refraction of attenuated waves in different media. In the field of GNSS based Geoscience research the group has contributed to region specific dislocation models in Sikkim Himalayas, Active deformation rates in Assam Valley and adjoining regions, Precipitable water vapor variability in Northeast India and Landslide deformation studies.

Inside

- ***Site response study in Bangalore city using H/V spectral ratio of microtremor***
- ***Reflection and refraction of attenuated waves at an imperfectly bonded interface between cracked elastic solid and porous solid saturated with two immiscible viscous fluids***
- ***Reflection and refraction of attenuated waves at the interface between cracked poroelastic medium and porous solid saturated with two immiscible fluids***
- ***Propagation of torsional surface in an inhomogeneous anisotropic fluid saturated porous double layers lying over gravitating dry sandy Gibson half space***

6.1 Crustal deformation models of Indian Himalayas and Indo-Burmese arc

Inverse Models have been developed for the Indian Himalayas from Ladakh in the west to Arunachal Himalaya in the east and the Indo-Burmese Arc. Horizontal surface deformation obtained from GPS time series for the past 20 years in these regions has been inverted to estimate the subsurface dislocation geometry and slip. These models have given constraints on the geometry of Main Himalayan Thrust and the varying slip in Ladakh, Garhwal, Kumaon, Nepal, Sikkim, Bhutan and Arunachal Himalaya. In the Indo-Burmese Arc these models point to segmentation of deformation along the North-South and East-West directions. For the first time surface deformation modelling has been carried out for the 2500 km stretch Himalayan Arc from west to east giving significant insights in to the seismic vulnerability of this major plate boundary which has a huge impact on the hazard assessment of this ecologically sensitive region

Sridevi Jade, Saigeetha Jagannathan, T S Shrungeshwara

6.2 Crustal strain, troposphere and ionosphere studies in Indian subcontinent

Continuous GPS(CGPS) data of a network of ~ 55 stations in the Indian continent for a period of 20 years (1995-2014) are analysed to obtain the time series of North, East and up displacements. These GPS time series are used to derive the strain accumulation across the Indian subcontinent thus delineating the zones of high stress buildup which is the main cause of earthquakes. Atmospheric delays obtained from the GPS analysis of CGPS sites is used to estimate the Integrated Water Vapor (IWV) and Total Electron Content (TEC) over the Indian subcontinent which is a crucial input to research related to GPS meteorology and ionosphere anomalies.

Sridevi Jade and T S Shrungeshwara

6.3 Region specific dislocation models in Darjiling-Sikkim Himalaya.

We used high-precision Global Positioning System (GPS) to geodetically constrain the motion of stations in the Darjiling-Sikkim Himalayan (DSH) wedge and examine the deformation at the Indian-Tibetan plate boundary using IGS (International GPS Service) fiducial stations. To obtain additional insight north of the Indo-Tibetan border and in the Darjiling-Sikkim-Tibet (DaSiT) wedge, published velocities from four stations J037, XIGA, J029 and YADO were also included in the analysis. India-fixed velocities or the back-slip was computed relative to the pole of rotation of the Indian Plate (Latitude 52.97 ± 0.22º, Longitude - 0.30 ± 3.76º, and Angular Velocity 0.500 ± 0.008º/ Myr) in the DaSiT wedge. Dislocation modelling was carried out with the back-slip to model the best possible solution of a finite rectangular dislocation or the causative fault based on dislocation theory that produced the observed back-slip using a forward modelling approach Three dislocation models (figure 6.1) were attempted and all the models simulate the frontal measured back-slip well. However, the one-dislocation model breaks down when we include velocities measured north of the Indo-Tibetan border . A two-dislocation model is needed to simu

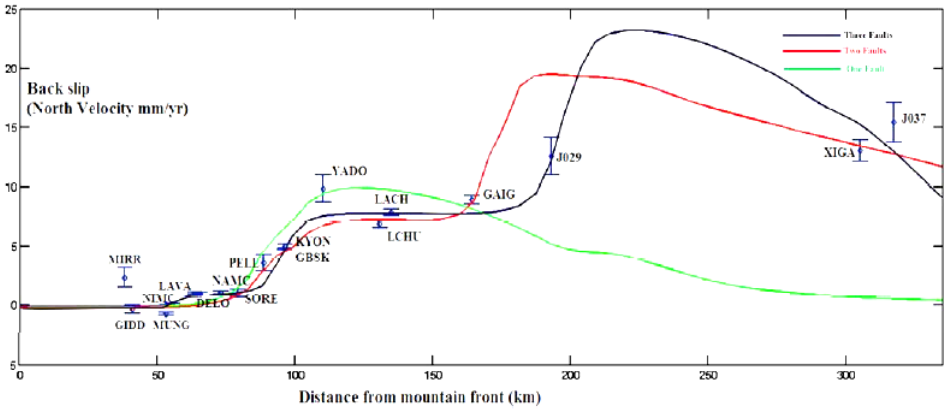

Figure 6.1 Modelled back-slip velocity for one-dislocation (green-line), two-dislocation (red-line) and three dislocation (black line) along with measured back-slip velocity of the GPS station

late the back-slip in the entire wedge. However, a three-dislocation model simulates the measured back-slip in the entire Darjiling-Sikkim-Tibet Himalayan wedge best (Figure 6.1).

A Kutubuddin, Malay Mukul, Sridevi Jade

6.4 GPS derived regional deformation rates in Assam Valley and Kopili fault

Northeast India is a seismo-tectonically complex and active region due to its unique location. GPS derived velocity field of northeast India quantifies the current status of the tectonic activity in Assam valley and Kopili fault area of northeast India. India fixed velocities of Assam valley indicate oblique deformation from west to east along the Assam valley. The GPS site velocities in the vicinity of Kopili fault indicate ~2 mm/yr dextral motion along Kopili fault. Results indicate strain accumulation in the valley with active deformation along Kopili fault. The slip of the Kopili fault is contributing to seismic moment accumulation (~70.74 X 10^{15} Nm/yr), sufficient to drive possible future earthquakes (Mw ≥ 5.17). The stressed Kopili fault region may witness future earthquakes thereby releasing the accumulated strain energy. GPS velocities indicate that the Assam valley may be fragmented along Kopili fault.

Prakash Barman, Sridevi Jade, Ashok Kumar

6.5 Integrated water vapor (IWV) variability over northeast India

Northeast India (Figure 6.2) has a unique geographical position which is bounded by the Himalayas and Tibetan plateau to the north, Bengal Basin to the south and Mishimi Hills to the east. The Patkoi-Naga-Chin-Arakan-Yoma (Indo-Myanmar) Hill ranges are situated in south east forming a North-South concave arc. The Shillong plateau and Mikir Hills are high rise areas of the region with elevation greater than 1000m over the Bangladeshi plains. Cherrapunji, located in Shillong plateau, is the world's wettest place and this is due to the unique orography of the region. The northeast India is the extreme north corner for the Indian monsoon flow where southwesterly moisture flow is confined to

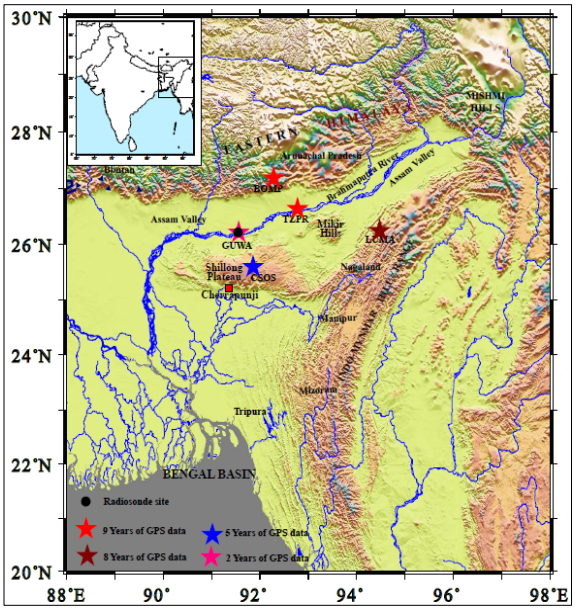

Figure 6.2 Orography of northeast India along with river system along with location of the GPS sites

Indian subcontinent by the Himalayas to the north and is directed westward. During monsoon, the region is badly flooded by the overloaded river Brahmaputra and its tributaries by the rain water of Bhutan and Arunachal Himalayas. In-depth study of GPS derived IWV variability water vapor over northeast India for a nine year period is carried out to better understand the rainfall pattern in this region leading to the flood hazard.

Prakash Barman, Sridevi Jade, Ashok Kumar

6.6 Present- day active deformation studies in Garhwal Himalayas

Garhwal Himalayas located in Uttarakhand is one of the most seismically active regions in the northwestern Himalayas. GPS time series (1996-2006) of this region indicate convergence of around 11mm/yr which is being accommodated in Lesser Himalaya just south of MCT (Main central Thrust) fault trace

Figure 6.3 Campaign survey GPS set-up at Sukhi, Uttarakhand

over a distance of 40-70 km. The Chamoli earthquake of 29th March 1999 with magnitude Mw6.5 *(*30.38° N, 79.21° E*)* occurred just south of the MCT fault trace in this region. Two GPS sites at Auli and Tungnath recorded both the co-seismic and post-seismic displacement of Chamoli earthquake. Auli and Tungnath baseline recorded an extension of 9 mm/yr which is due to the post-seismic relaxation of the Chamoli earthquake. GPS remeasurements were carried out in 2014 for all the GPS sites in Garhwal Himalaya to quantify the present-day active deformation in this region.

T S Shrungeshwara, N R Pavithra, G Chiranjeevi Vivek , Sridevi Jade and CBRI team

6.7 Landslide deformation studies in Uttarakhand, India

Large number of slope failures have been triggered on the main highways in Garhwal Himalayas since Chamoli earthquake of 6.6 magnitude in 1999. Over the years, one such National Highway from Chamoli to Badrinath along the river Alaknanda is majorly affected due to landslides in Uttarakhand region. The upstream part of Alaknanda River often

Figure 6.4 Continuous GNSS station at CSIR-CBRI Roorkee

triggers landslides especially during rainy seasons. Several landslides were triggered along this highway during the 2013 cloud burst in this region The landslides along this National Highway are mostly debris slides or rock slides. As part of this study, CSIR-Central Building Research Institute (CBRI) in collaboration with CSIR-4PI selected two landslides in Jalgwar village, Chamoli district, Uttarakhand. The selected landslide in Jalgwar village is situated with in latitude 30.45 N – 30.48 N to longitude 79.44 E – 79.47 E. GPS measurements were carried out in October 2014, January 2015 and March 2015 to monitor the landslide movement.

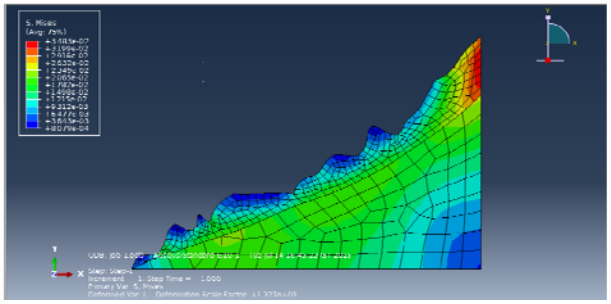

Figure 6.5 Schematic representation of the slide of soil in the landslide due to various loads acting over it

The data were analyzed using GAMIT/GLOBK software and Track - GPS differential phase kinematic positioning program to calculate position estimates of landslide points treated as kinematic stations along with nearby static reference stations. Position estimates calculated by the track program and these positions over a period of time are used for calculating the strain rates between the points. Preliminary estimates show shortening of baselines for landslide 1 indicating the relative motion within the landslide is convergence. For landslide 2 there is extension of baselines between the landslide points indicating the sense of motion within the landslide. Along with the geodetic measurements an effort has been initiated to model the landslides using Finite Element Modelling technique along with various geotechnical parameters such as pore water pressure, permeability co-efficient, Mohr's- Coulomb criteria and Principal stresses. In addition continuous GNSS station is established in March 2015 at CBRI campus, Roorkee to serve as a reference site to constrain deformation south of frontal Himalaya.

T S Shrungeshwara, G Chiranjeevi Vivek, N R Pavithra, A K Dharma Teja, Sridevi Jade & CBRI team

6.8 Seismic hazard and risks assessment based on the Unified Scaling Law for Earthquakes

The Unified Scaling Law for Earthquakes, USLE, that generalizes the Gutenberg-Richter recurrence relation, has evident implications since any estimate of seismic hazard depends on the size of territory that is used for investigation, averaging, and extrapolation into the future. Therefore, the hazard may differ dramatically when scaled down to the proportion of the area of interest (e.g. a city) from the enveloping area of investigation. In fact, given the observed patterns of distributed seismic activity the results of multi-scale analysis embedded in USLE approach demonstrate that traditional estimations of seismic hazard and risks for cities and urban agglomerations are usually underestimated. More

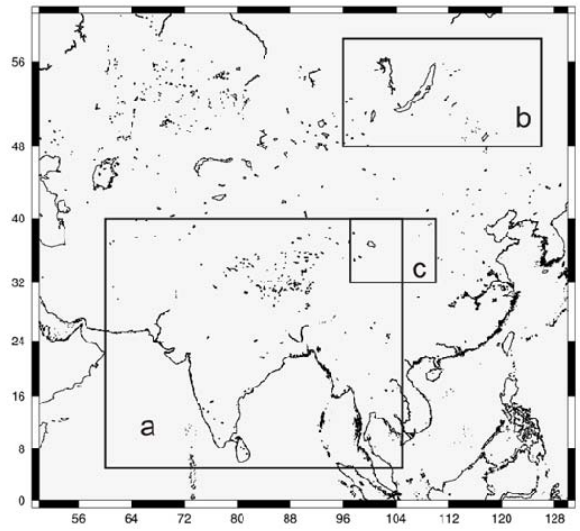

Figure 6.6 The three regions: the Himalayas and surroundings (a), Lake Baikal (b) and Central China (c).

over, the USLE approach provides a significant improvement when compared to the results of probabilistic seismic hazard analysis, e.g. the maps resulted from the Global Seismic Hazard Assessment Project, GSHAP. In this paper, we apply the USLE approach to evaluating seismic hazard and risks to population of the three territories of different size representing a sub-continental and two different regional scales of analysis – i.e. the Himalayas and surroundings, Lake Baikal, and Central China regions (Figure 6.6).

The USLE coefficients were used for estimation and mapping the expected maximum magnitude *Mmax* with a 10 % chance of exceedence in 50 years specifically, for each 0.5° × 0.5° cell at seismic location on a regional map (Figure 6.7). Figure 6.8 shows the three regional seismic hazard maps in terms of Peak Ground Acceleration (PGA) determined for each grid point from a source of *Mmax.* The maximum of acceleration values computed at a grid point is assigned to it. We have opted the minimum and maximum distances of 10 and 500 km, respectively. There exist many different risk esti-

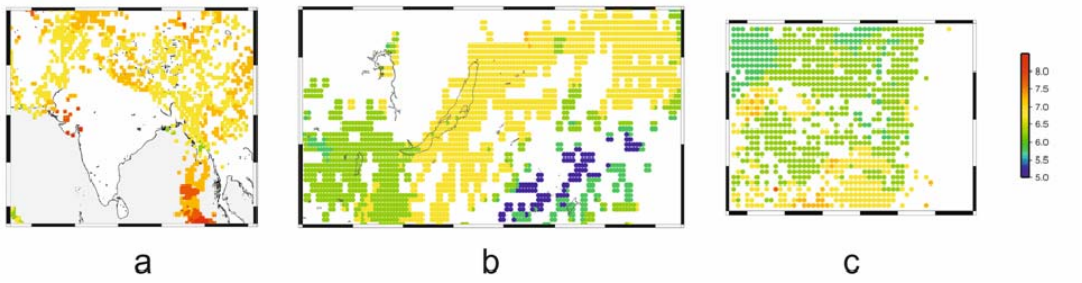

Figure 6.7 The seismic hazard maps for the three regions in terms of *Mmax*: the Himalayas and surroundings (a), Lake Baikal (b), and Central China (c)

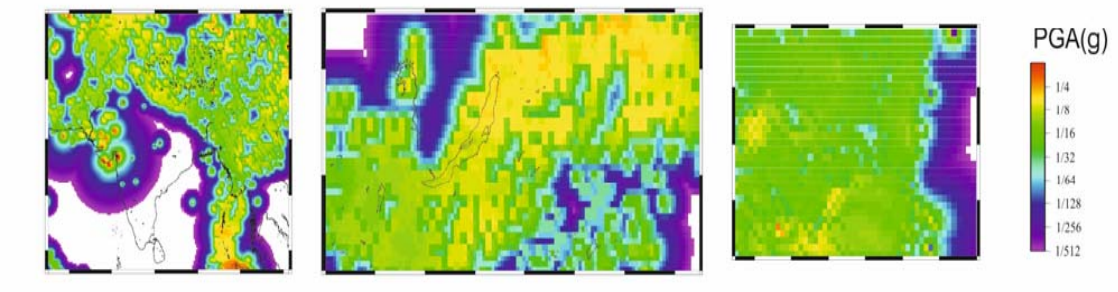

Figure 6.8 The seismic hazard maps for the three regions in terms of PGA (in g) based on USLE approach: the Himalayas and surroundings (a), Lake Baikal (b), and Central China (c)

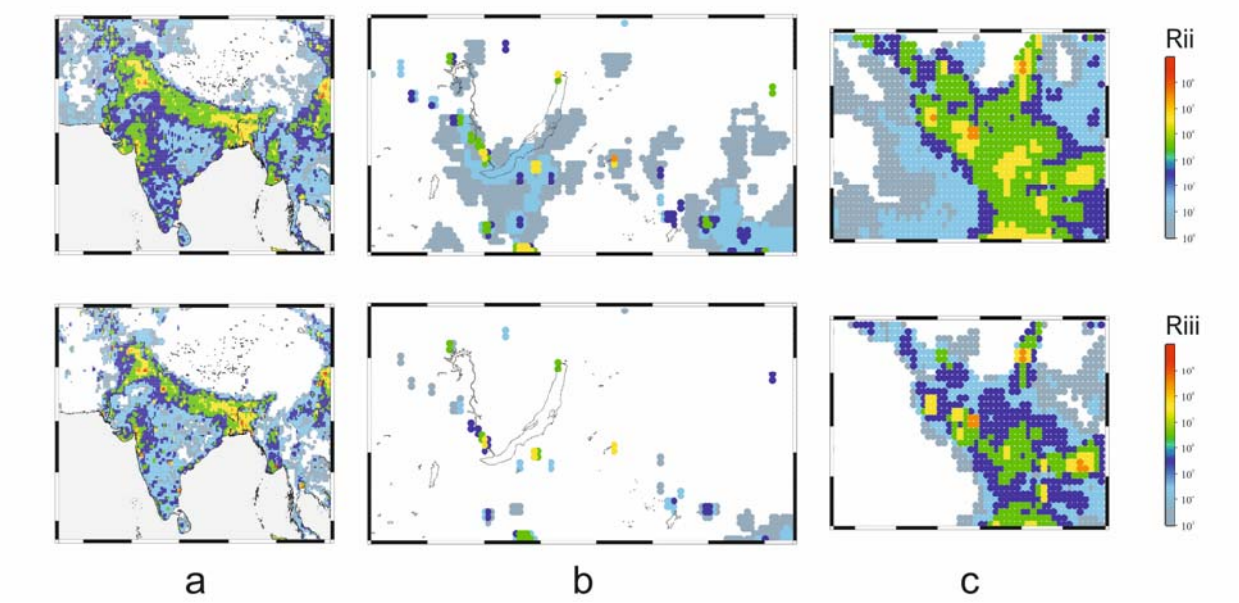

Figure 6.9 The maps of seismic risk for population of the three regions: the Himalayas and surroundings (a), Lake Baikal (b), and Central China (c). Oversimplified convolutions of seismic hazard map H(g) with the population density distribution P: Rii (g) = H(g) · ∫gP · P (upper row) and Riii (g) = H(g) · ∫gP · P_2 (bottom row).

mates even if the same object of risk and the same object of risk and the same hazard are involved. The variety may result from the different laws of convolution, as well as from different kinds of vulnerability of an object of risk under specific environments and conditions. Both the conceptual issues must be resolved in a multidisciplinary problem oriented research performed by specialists in the fields of hazard, objects of risk, and object vulnerability. To illustrate the concept, we perform the two oversimplified convolutions of seismic hazard assessment map based on USLE with the population density. The resulting maps of the two risks in arbitrary units are given in Figure 6.9. The first estimate in a cell g is based on the individual vulnerability in proportion to the population density at a given site, Rii (g) = H(g) · ∫gP · P, where ∫gP is the integral of the population density over the cell g, i.e. the number of individuals within the area of the cell g. The second risk estimate is Riii (g) = H(g) · ∫gP · P^2. Both appear to be rather natural due to specifics of man-made environment inflicted in the areas of high concentration of individuals. To avoid misleading interpretations, we have to emphasize that the risk estimates presented for the three regions under study are given for academic methodological purposes only.

Anastasia Nekrasova* Imtiyaz A Parvez, Vladimir Kossobokov* and X Tao**
*Institute of Earthquake Prediction Theory & Mathematical Geophysics, RAS, Moscow
**Harbin Institute of Technology, People's Republic of China.

6.9 Crustal Structure beneath Kashmir Himalaya: A preliminary estimation from five broadband stations

An attempt has been made to map the detachment plane in Kashmir Himalaya to identify possible asperities that would allow a more realistic modelling of seismic hazard in the region. The results presented here constitute the first information about a consistent Moho geometry of the region even as we densify the network to attempt high-resolution images of the Moho and the overlying décollement.

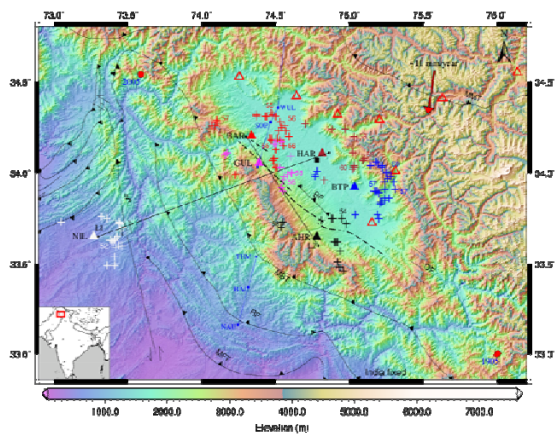

Figure 6.10 Shows map of Kashmir Valley and adjacent areas. Hollow red triangles are the stations which are to be installed; others are the stations (BAR, GUL, AHR, BTP and NIL) whose data were used in this study. NIL (white triangle at bottom left) is the IRIS station in Nilore Pakistan. Crosses are piercing points representing upcoming Ps converted phases at Moho for respective station (color match). Figures near to piercing points are Moho depths from forward modelling.

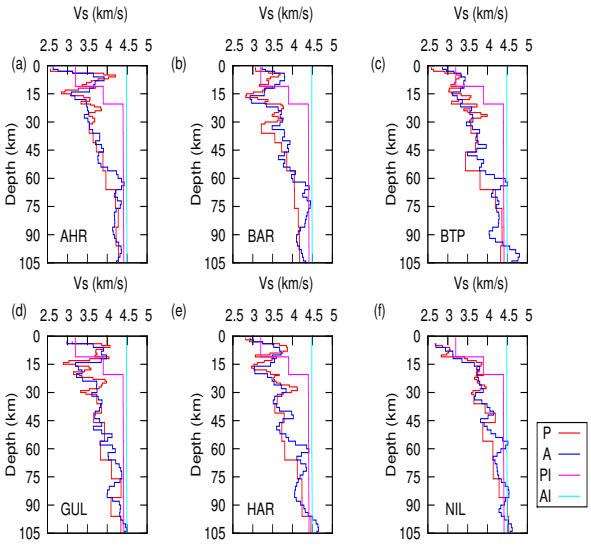

Figure 6.11 Shows comparison of inversion using AK135 and PREM models for all stations. We see a LVZ beneath all except NIL, P means inversion using PREM model and A means inversion using AK135 model. AI=AK135 initial model and PI=PREM initial model.

We investigate the crustal structure beneath the intermountain Kashmir valley carved within the Great Himalaya by the differential uplift of its south-western part, which constitutes the northern Pir Panjal ranges. The data for our analysis comes from five broadband seismic stations located on hard rock sites of the valley, three on its south-western and two adjoining its north-eastern edges. Four Guralp 3TD broadband seismic sensors were operated at bedrock sites (Figure 6.10 AHR, BAR, BTP and GUL) from June 2013 to June 2014, and a fifth Nanometrics Trillium 120P seismometer at HAR close to Srinagar from September to November 2014. Additionally, we use the data from the IRIS station at Nilore (NIL) in Pakistan. For the present analysis, we use data pertaining to all M>6 earthquakes in the epicentral range of 30 to 100 degrees, and selected only the high quality records. Data at all these stations were recorded continuously at a sample rate of 100 samples per second and time stamped using a GPS receiver at all the stations.

Receiver Functions (RFs) at these sites were calculated using the iterative time domain deconvolution method and jointly inverted with surface wave dispersion data to estimate the shear wave velocity structure beneath each station. To enhance the signal to noise ratio of the weak conversions, receiver functions were stacked in small bins of close backazimuth and delta values. This enhances discrimination between lateral variations within stations. Furthermore, a tight stacking of RFs with Backazimuth BAZ $\leq$ 8° and delta $\leq$ 5° obviates the blurring of stacks because of attenuation in Ps phases and facilitates identification of later reverberations. To further test the results of inversion (figure 6.11), we applied forward modelling by dividing the crust beneath each station into 4-6 homo-

geneous, isotropic layers. Moho depths were separately calculated for closely spaced clusters of Moho piercing points from the inversion of high quality stacked receiver functions pertaining to these piercing point. Their uncertainties were further constrained within ±2 km by trial forward modelling as Moho depths were varied over a range of ±6 km in steps of ±2 km and the synthetic receiver functions matched with the inverted ones. The final values were also found to conform to those independently estimated using the H-K stacks. The Moho depths on the south-western edge of the valley are close to 55 km, but increase to about 58 km towards the eastern edge, suggesting that here, as in the central and Nepal Himalaya, the Indian plate dips northeastwards beneath the Himalaya. We also calculated the V_p/V_s ratio beneath these 5 stations which were found to lie between 1.7 and 1.76, yielding a Poisson's ratio of ~0.25 which is characteristic of a felsic composition.

Ramees R Mir, Imtiyaz A Parvez, Vinod K Gaur, Ashish, Rakesh Chandra* and Shakil A Romshoo*
*University of Kashmir, Srinagar

6.10 Probabilistic earthquake hazard assessment for Peninsular India

Peninsular India, usually considered as a stable continental part of the Indian subcontinent, has experienced damaging earthquakes of magnitude ~6 and more in the last couple of decades. Earthquakes occurred in various places in Peninsular India: Latur (1993, Mw 6.1), Jabalpur (1997, Mw 5.8) and most recently Bhuj (2001, Mw 7.6), claiming thousands of lives and causing huge economic losses due to the dam- age to infrastructure. Although the frequency of occurrence of large earthquakes is low, their impact on society is high. Thus, it becomes important to quantify the seismic hazard for Peninsular India for future events in terms of potential ground shaking, while at the same time acknowledging difficulties and the inherent uncertainties. The seismicity and major geological features are illustrated in Figure 6.12.

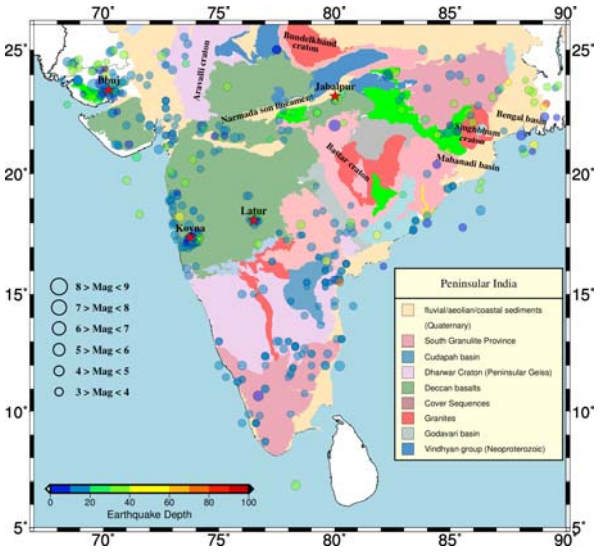

Figure 6.12 Geology of Peninsular India derived from the Geological Map India (GSI, 2000), and locations of historical earthquakes (circles). Colour and diameter of circles indicate depth and magnitude, respectively. Red stars indicate major events that occurred during the past 50 years.

In this paper, a new probabilistic seismic hazard assessment (PSHA) is presented for Peninsular India. The PSHA has been performed using three ferent recurrence models: a classical seismic zonation model, a fault model and a grid model. The development of a grid model based on a non-parameterised recurrence model using an adaptation of the Kernel based method that has not been applied to this region before. The results obtained from the three models have been combined in a logic tree structure in order to investigate the impact of different

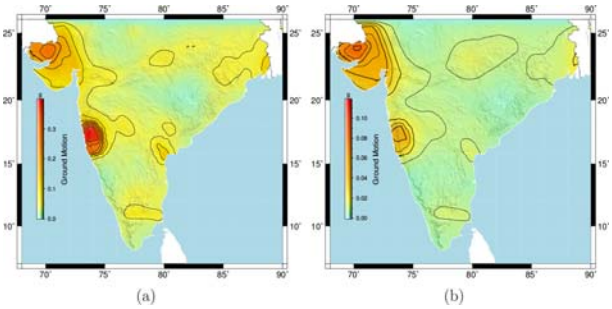

Figure 6.13 Hazard maps computed for 10% probability of exceedance in 50 years (return period 475 years), using a logic tree approach with equal weights for all three seismicity models; displayed at (a) PGA and (b) a spectral acceleration of 1 Hz; see colour bar for values.

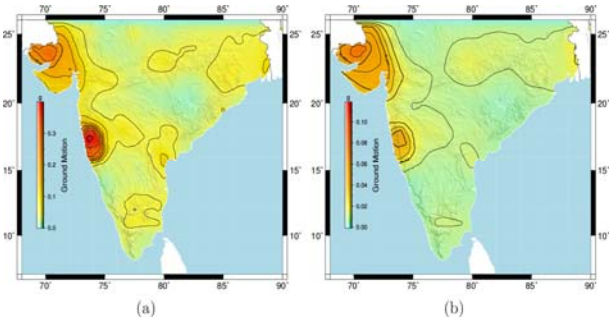

Figure 6.14 Hazard maps computed for 10% probability of exceedance in 50 years (return period 475 years), using a logic tree approach with weights of 0.4, 0.2 and 0.4 for the zonation, fault and grid model, respectively; displayed at (a) PGA and (b) a spectral acceleration of 1 Hz; see colour bar for values.

weights of the models. Three suitable attenuationrelations have been considered in terms of spectral acceleration for the stable continental crust as well as for the active crust within the Gujarat region. While Peninsular India has experienced large earthquakes e.g. Latur and Jabalpur, it represents in general a stable continental region with little earthquake activity, as also confirmed in our hazard results.

On the other hand, our study demonstrates that both the Gujarat and the Koyna regions are exposed to a high seismic hazard (Figures 6.13 and 6.14). The peak ground acceleration for 10% exceedance in 50 years observed in Koyna is 0.4 g and in the Kutchh region of Gujarat up to 0.3 g. With respect to spectral acceleration at 1 Hz, estimated ground motion amplitudes are higher in Gujarat than in the Koyna region due to the higher frequency of occurrence of larger earthquakes. We discuss the higher PGA levels for Koyna compared Gujarat and do not accept them uncritically.

Ashish, Daniela Kuehn*, Conrad Lindholm* and Imtiyaz A Parvez
*NORSAR, Norway

6.11 Site response study in Bangalore city using H/V spectral ratio of Microtremor

Bangalore a highly developed and dense city, also the capital of Karnataka is situated in the Peninsular Deccan plateau of India. The seismicity level of Bangalore is low to moderate and it lies in seismogenic zone II. There are no frequent earthquakes reported in Bangalore and surrounding area except that the city has felt in 1900 Coimbatore earthquake (M=6.0). However, due to high alteration of soil structure such as dried up lakes for erosion and encroachment, it becomes a matter of interest for scientists how these buildings (constructed on sedimentary deposits) will react to any moderate/large earthquake. We have estimated the site responses at the Bangalore city using the single station spectral ratio method widely known as H/V spectral ratio technique. For computation of the spectral ratio using Nakamura's method, the GEOPSY software has been used. This spectral ratio provides a good estimate of the fundamental frequency of the site although the site amplification factor is over estimated. Site response analysis is a fundamental part

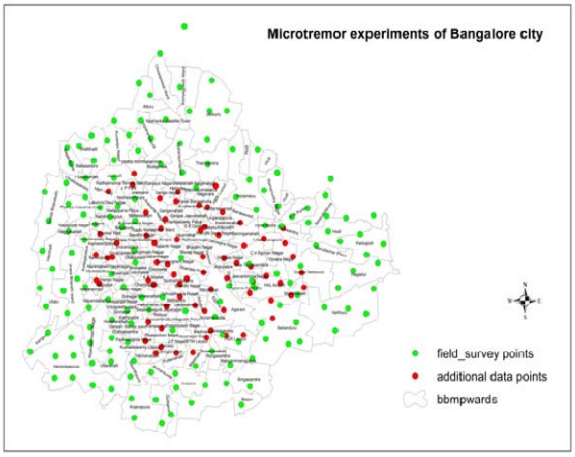

Figure 6.15 The location of sites for microtremor data collection in Bangalore city

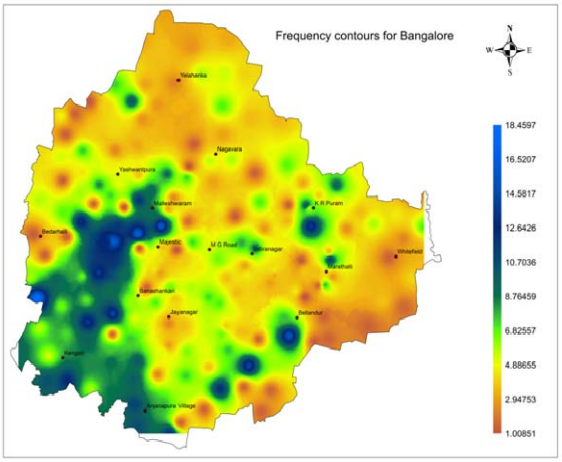

Figure 6.16 Distribution of fundamental frequency (f0) estimated from H/V spectral ratio using Nakamura's technique.

of assessing seismic hazard in earthquake prone areas. Although there are number of methods to evaluate seismic hazard, but due to its low cost and simplicity, ambient seismic noise (microtremor) measurement is preferred by many. Microtremors are short period vibrations that result from human activity (traffic, machinery), atmospheric loading, wind etc. The main objective of this project is to compute the horizontal to vertical spectral ratio (H/V ratio) using Nakamura's technique, which generates the peak period fundamental frequency. In addition, on soft soil sites, where contrast is high between bedrock and top soil they usually exhibit a clear peak that is well correlated with the fundamental resonant frequency. It is now commonly accepted in the earthquake engineering community that soft soils can play a large role in ground motion and must be included in seismic zoning. The phenomenon responsible for the amplification of the ground motion in areas with soft sediments is the trapping of seismic waves within sediments due to acoustic impedance contrast between sediment and bedrock. The interference of these trapped waves leads to resonances whose shapes and frequencies are well correlated with geometrical and mechanical characteristics of the structure.

For this study more than 200 single station ambient noise measurements (Figure 6.15) are performed and the data is processed. The predominant frequencies surveyed in Bangalore city range between 1.0~18 Hz and it is found that they are higher in the southwest part compared to southeast part (Figure 6.16). Comparing them with the overburden thickness inferred from various borehole locations validates the reliability of the result. The resonant frequency obtained from the observations correlated very well with the one obtained from soil thickness and shows extensive lateral variation in soft sediments thickness. The mapping of resonant frequency permits identification of zones at risk. It can be used as a tool for prevention, planning and retrofitting measures, also to define safety zones for reconstruction after a destructive earthquake.

Imtiyaz A Parvez, Reshma Bhat, Haseeb Rehman, Bhavani Kambala and Prajith KC

6.12 Reflection and refraction of attenuated waves at an imperfectly bonded interface between cracked elastic solid and porous solid saturated with two immiscible viscous fluids

The present study describes the propagation of elastic waves across the imperfectly bonded interface between the cracked elastic solid and porous solid saturated with two immiscible viscous fluids. We assume that both the media are loosely connected to each other and the connected coefficient or bonding parameter is represented here by ψ. The interface between these two media is assumed at $x_3 = 0.$

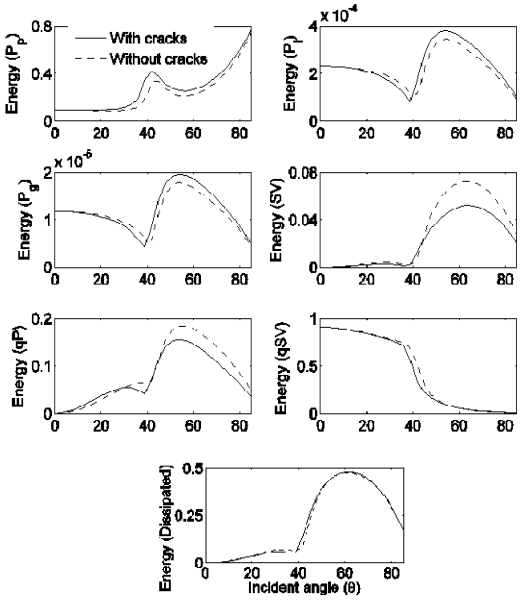

Figure 6.17 Energy shares of incident P_p wave by the reflected (P_p, P_l, P_g, SV) waves, refracted (qP, qSV) waves and energy dissipation at the interface $x_3 = 0$ with incidence direction θ for presence and absence of the cracks in elastic half space.

We solve the dynamical equations with the help of the assumed harmonic solution. The obtained results are in the form of Christoffel equations and these results provide four inhomogeneous waves in a porous medium, of which three are longitudinal waves and one is a transverse wave. The reflection coefficients and energy share have been solved for given boundary conditions at a loosely bounded interface. The energy matrix defines the distribution of the incident energy to the four reflected waves, two refracted waves and some energy is lost at the interface and is defined as dissipation energy. The final results related to energy share satisfy the conservation law of energy. We have also conducted a comparative study between the presence and absence of vertical aligned cracks in the elastic half space. For the numerical validation of the present study, we assume that the first medium is water and CO_2 saturated sandstone and second medium is basaltic rock. From figure 6.17, we find that the vertically aligned cracks in the elastic half space give significant deference in the energy share of the incident wave by reflected and refracted waves. In the absence of the cracks, less energy will be absorbed at the loosely bounded interface in the form of dissipated energy.

Sushant Shekhar and Imtiyaz A Parvez

6.12 Reflection and refraction of attenuated waves at the interface between cracked poroelastic medium and porous solid saturated with two immiscible fluids

The present study generalizes the study of the previous problem in which we assume that the poroelastic solid saturated with two immiscible fluids is in contact with the cracked poroelastic solid with sin-

gle fluid at x_3= 0. We assume that viscosity is present in both media. To solve these elastodynamic equations, we have used the Helmholtz technique for finding the harmonic solutions. In the process, scalar potentials provide five longitudinal waves and vector potentials provide two transverse wave for both media. The inhomogeneous propagation of the incident wave, reflected waves and refracted waves are specified through the respected propagation directions and attenuation directions. The incident wave propagates through the cracked poroelastic solid and is incident at a point on the interface x_3= 0 result as three reflected waves and four refracted waves. The energy matrix defines the distribution of incident energy to the three reflected waves, four refracted waves and some of the energy will be spent on the interaction of the waves with each other. The final results related to energy share satisfy the conservation law of energy.

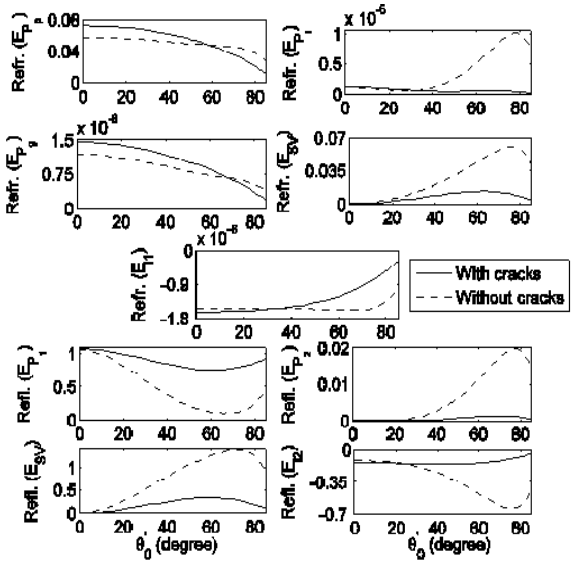

Figure 6.18 Energy shares of incident P_p wave by the refracted (P_p, P_l, P_g, SV) waves, reflected (P_1, SV) waves and the interaction energies E_{l1} and E_{l2} at the interface $x_3 = 0$ with incidence direction $\theta_0^{'}$ for presence and absence of the cracks in poroelastic half space.

For a given incident P_l wave, the presence of cracks in the poroelastic solid has significant effects on the energy share of the incident wave by reflected, refracted and the interaction energies E_{l1}, E_{l2} see figure 6.18. The energy shares of refracted slow P_i and P_g waves are very small in comparison to other energy shares.

Sushant Shekhar and Imtiyaz A Parvez

6.13 Propagation of torsional surface in an inhomogeneous anisotropic fluid saturated porous double layers lying over gravitating dry sandy Gibson half space

We try to determine the existence of torsional surface waves in inhomogeneous fluid saturated second porous layer lying in between an inhomogeneous fluid saturated first porous layer and an inhomogeneous dry sandy Gibson half space under initial stresses. Based on the previous available literature it is clear that in the crust different inhomogeneities are available from place to place. In the present study, we assume that the inhomogeneity varies in both of the porous layers quadratically and exponentially in rigidity, density and initial stress and in the Gibson half space, inhomogeneity varies linearly in rigidity and initial stress. We use the separation of variable technique for solving the dynamical equations. We consider a numerical example for the validation of the proposed model, namely a water saturated limestone layer sandwiched in between a kerosene saturated sandstone and a dry sandy half space

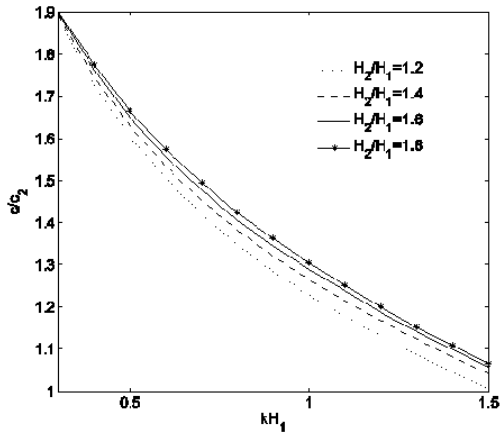

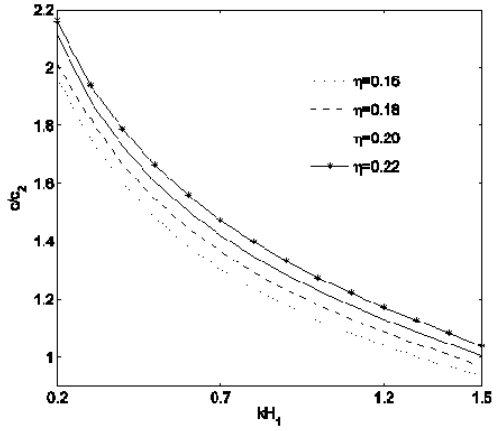

Figure 6.19 Variation of the dimensionless phase velocity (c/c_2) with dimensionless wave number kH_1 for given values of (a) width ratio (H_2/H_1), (b) sandy parameter η.

(Gibson half space). The phase velocity of torsional surface waves in sandwiched layer (second porous layer) is computed numerically. From the present study it is clear that:

(1) The width of the porous layer plays an important role in the study of torsional surface waves.

(2) The sandy parameter η that represents dry sandy Gibson half space has a significant effect on phase velocity of torsional surface waves (Figure 6.19).

Sushant Shekhar and Imtiyaz A Parvez